BMB
Reports

BMB Rep. 2018; 51(2): 79-84
www.bmbreports.org

The role of Purkinje cell-derived VEGF in cerebellar astrogliosis in Niemann-Pick type C mice

Min Hee Park[1,2,3], *Ju Youn Lee*[1,2,3], *Min Seock Jeong*[1,4], *Hyung Sup Jang*[1,4], *Shogo Endo*[5], *Jae-sung Bae*[1,2,3,*] & *Hee Kyung Jin*[1,4,*]

[1]Stem Cell Neuroplasticity Research Group, Kyungpook National University, Daegu 41566, [2]Department of Physiology, Cell and Matrix Research Institute, School of Medicine, Kyungpook National University, Daegu 41944, [3]Department of Biomedical Science, BK21 Plus KNU Biomedical Convergence Program, Kyungpook National University, Daegu 41944, [4]Department of Laboratory Animal Medicine, College of Veterinary Medicine, Kyungpook National University, Daegu 41566, Korea, [5]Aging Neuroscience Research Team, Tokyo Metropolitan Institute of Gerontology, Tokyo 173-0015, Japan

Niemann-Pick type C disease (NP-C) is a fatal neurodegenerative disorder caused by a deficiency of *NPC1* gene function, which leads to severe neuroinflammation such as astrogliosis. While reports demonstrating neuroinflammation are prevalent in NP-C, information about the onset and progression of cerebellar astrogliosis in this disorder is lacking. Using gene targeting, we generated vascular endothelial growth factor (VEGF) conditional null mutant mice. Deletion of VEGF in cerebellar Purkinje neurons (PNs) led to a significant increase of astrogliosis in the brain of NP-C mice in addition to the loss of PNs, suggesting PN-derived VEGF as an important factor in NP-C pathology. Moreover, replenishment of VEGF in neurons improved brain pathology in NP-C mice. Overall, our data provide a new pathological perspective on cerebellar astrogliosis in NP-C and suggest the importance of VEGF as a therapeutic target for this disease. [BMB Reports 2018; 51(2): 79-84]

INTRODUCTION

Niemann Pick Type-C disease (NP-C) is an autosomal recessive disorder characterized by liver disease, lung disease, and neurodegeneration, which lead to premature death (1, 2). In NP-C, the cerebellum, which is the major site of NP-C pathology, exhibits a significant accumulation of gangliosides and sphingolipids, as well as axonal abnormalities and motor dysfunction (2-4). NP-C is also characterized by neurodegeneration, including patterned loss of cerebellar Purkinje neurons (PNs) and neuroinflammation (5).

Neuronal death occurs progressively in NP-C disease, affecting cerebellar PNs in particular (2). In addition, dysfunction of non-neuronal cells in the brain, such as astrocytes and microglia, has been proposed to contribute to the NP-C related neurodegeneration (6). Recently, we have found that vascular endothelial growth factor (VEGF) activity is reduced in NP-C neurons, causing the loss of PNs. Increase of brain specific-VEGF also improved NP-C pathology, including PNs survival, motor function, and lifespan, implying that VEGF derived from PNs is an important factor in regulating NP-C pathogenesis. However, this study did not assess the role of VEGF derived from PNs on the inflammatory response, known to be a main feature in NP-C. In the present study, we focused on the role of PNs-derived VEGF in NP-C associated neuroinflammation using conditional knockout mice with PNs-specific loss of VEGF and NP-C mice with neuron-specific VEGF overexpression. Our results prove that the level of VEGF in PNs is the main contributor to astrogliosis in the cerebellum of NP-C mice. Thus, we provide evidence that VEGF is required for the regulation of neuroinflammatory response and suggest that VEGF might be an important target for treatment of NP-C.

RESULTS

Appearance of NP-C phenotype after *NPC1* gene deletion on PNs

We first sought to determine the extent to which cell autonomous toxicity shows an NP-C phenotype. To achieve PN-specific deletion of *NPC1*, we used L7/Pcp2-cre mice, in which the expression of Cre recombinase is limited to cerebellar PNs (7). L7/Pcp2-cre mice were crossed with *NPC1*$^{flox/flox}$ mice to drive *NPC1* gene deletion in PNs (Fig. 1A). We first assessed the motor function/coordination using the Rota-rod test. L7/Pcp2-cre;*NPC1*$^{flox/flox}$ mice showed a significant decrease of motor function/coordination (Fig. 1B), similar to a

*Corresponding authors. Jae-sung Bae, Tel: +82-53-420-4815; Fax: +82-53-424-3349; E-mail: jsbae@knu.ac.kr; Hee Kyung Jin, Tel: +82-53-950-5966; Fax: +82-53-950-5955; E-mail: hkjin@knu.ac.kr

https://doi.org/10.5483/BMBRep.2018.51.2.168

Received 26 August 2017, Revised 16 September 2017, Accepted 20 October 2017

Keywords: Cerebellar astrogliosis, Niemann-Pick type C disease, Purkinje neuron, Vascular endothelial growth factor

ISSN: 1976-670X (electronic edition)

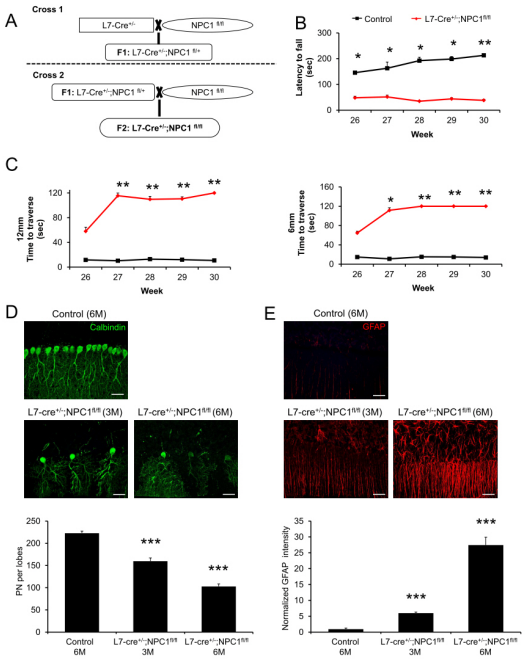

Fig. 1. Phenotype and pathology following PNs- specific deletion of *NPC1*. (A) Generation of L7/Pcp2-cre;*NPC1*$^{flox/flox}$ mice. (B) Rota-rod scores of control and L7/Pcp2-cre;*NPC1*$^{flox/flox}$ mice (n = 6-7 per group). (C) Beam test of control and L7/Pcp2-cre;*NPC1*$^{flox/flox}$ mice. Left, 12-mm square beam. Right, 6-mm square beam (n = 6-7 per group). (D) Confocal images and quantification of cerebellar PNs in control and L7/Pcp2-cre;*NPC1*$^{flox/flox}$ mice (IV and V lobes, n = 3-4 per group). Scale bars, 50 μm. (E) Representative confocal images and quantification of astrocytes activation in control and L7/Pcp2-cre;*NPC1*$^{flox/flox}$ mice (n = 3-4 per group). Scale bars, 50 μm. (B-E) Student's t test. *P < 0.05, **P < 0.01, ***P < 0.001. All error bars indicate standard error of the mean.

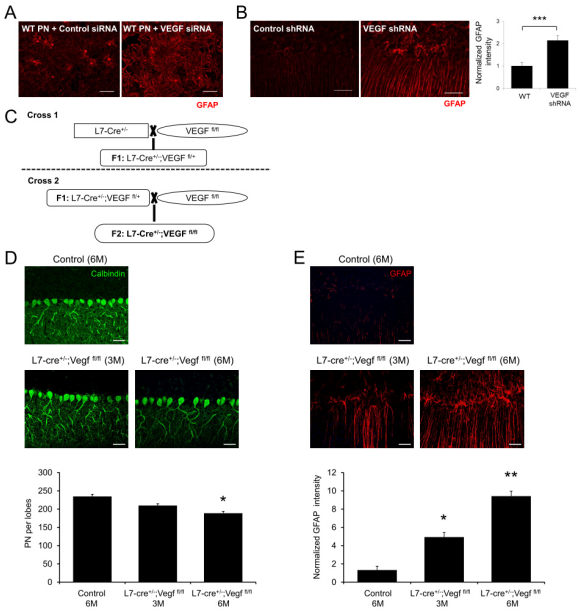

Fig. 2. Effect of PNs specific deletion of VEGF on PNs survival and neuroinflammation. (A) Representative confocal images of astrocytes activation in cultured cerebellar cells after VEGF siRNA treatment. Scale bar, 50 μm. (B) Representative fluorescence images and quantification of GFAP in VEGF shRNA treated mice cerebellum (n = 3 per group). Scale bars, 50 μm. (C) Generation of L7/Pcp2-cre;VEGF$^{flox/flox}$ mice. (D) Confocal images and quantification of cerebellar PNs in control and L7/Pcp2-cre;VEGF$^{flox/flox}$ mice (IV and V lobes, n = 3-4 per group). Scale bars, 50 μm. (E) Representative confocal images and quantification of astrocytes activation in control and L7/Pcp2-cre;VEGF$^{flox/flox}$ mice (n = 3-4 per group). Scale bars, 50 μm. (B, D, E) Student's t test. *P < 0.05, **P < 0.01, ***P < 0.001. All error bars indicate standard error of the mean.

previous report (8). Limb coordination and balance were also measured with the balance beam test. L7/Pcp2-cre;*NPC1*$^{flox/flox}$ mice took longer to transverse the beams compared with age-matched control mice (Fig. 1C). These results showed that NPC1 deficiency in PNs is sufficient to cause disruption of motor function/coordination. Because the degeneration of PNs is generally known in NP-C brain pathology, we quantified the cerebellar PNs survival in PNs-specific null mice by immunofluorescence using anti-calbindin antibody. L7/Pcp2-cre;*NPC1*$^{flox/flox}$ mice showed a significant loss of PNs at 3 months of age, which was further exacerbated in 6 month-old L7/Pcp2-cre;*NPC1*$^{flox/flox}$ mice (Fig. 1D). Another indicator of brain pathology in NP-C is excessive inflammation. To investigate whether PNs specific loss of NPC1 affect neuroinflammation, we examined astrocyte activation in mice using glial fibrillary acidic protein (GFAP) staining. Astrocyte activation was significantly higher in brains of L7/Pcp2-cre;*NPC1*$^{flox/flox}$ mice compared with those of control mice, and was more severe with aging (Fig. 1E). Taken together, these data indicate that depletion of *NPC1* gene in cerebellar PNs causes NP-C pathology including motor dysfunction, loss of PNs, and astrogliosis.

The effects of VEGF gene deletion on PNs

VEGF, which has been described as an endothelial cell specific mitogen, also affects neuronal survival and neuroinflammation (9, 10). Moreover, our previous study reported that mutated *NPC1* in PNs caused a decrease in VEGF levels and led to sphingosine accumulation, resulting in neuronal dysfunction (2). To determine whether VEGF level in PNs mediates neuroinflammation, we cultured primary cerebellar cells including PNs and astrocytes. Compared with control cells, astrocyte activation was significantly higher in the VEGF siRNA treated cells (Fig. 2A). Similarly, direct injection of VEGF shRNA into the cerebellum of wild-type (WT) mice led to severe astrogliosis (Fig. 2B). These data showed that reduction of VEGF levels contributed to abnormal gliosis in the cerebellum, suggesting an important effect of VEGF on

gliosis in the NP-C microenvironment. To assess the effects of PN-derived VEGF on neuroinflammation more specifically, we generated L7/Pcp2-cre;VEGF$^{flox/flox}$ mice (Fig. 2C). The L7/Pcp2-cre;VEGF$^{flox/flox}$ mice, which are conditional knockout mice lacking VEGF in PNs, showed a decrease of PN survival and upregulation of astrocyte activation (Fig. 2D, E) at 3 months, and these were accelerated further at 6 months of age (Fig. 2D, E). Similar to the data of *NPC1* deletion in PNs, our results showed that inactivation of VEGF in PNs also evokes NP-C symptoms, such as PN loss and astrogliosis, suggesting the importance of VEGF in NP-C pathogenesis.

Improvement of NP-C pathology by replenishment of VEGF

To assess whether the increase of VEGF improves NP-C brain pathology including astrogliosis, neuronal-specific VEGF overexpressing transgenic mice were bred with NP-C mice (Fig. 3A). Compared with cerebellar cells derived from WT mice, cells derived from NP-C mice showed significantly increased astrocyte activation (Fig. 3B). These were significantly decreased in cells derived from VEGF/NP-C mice (Fig. 3B). Furthermore, to investigate changes of astrocyte activation, we used brain samples. As expected, the astrocyte activation was significantly higher in the cerebellum of NP-C mice compared with WT mice, but was decreased in brains of VEGF/NP-C mice (Fig. 3C, D). Moreover, we observed an elevation of inflammation activating cytokines in the NP-C mice, and correction of these cytokines in the VEGF/NP-C mice (Fig. 3E). Finally, VEGF/NP-C mice showed a slight improvement of motor function/coordination compared with NP-C mice (Fig. 3F, G). We have previously reported that PN survival was significantly improved in VEGF/NP-C mice compared with NP-C mice (2). Taken together, our results indicate that neuronal VEGF overexpression exerts a therapeutic effect by regulating the inflammatory response in NP-C mice, suggesting that VEGF could be a potential therapeutic target for NP-C.

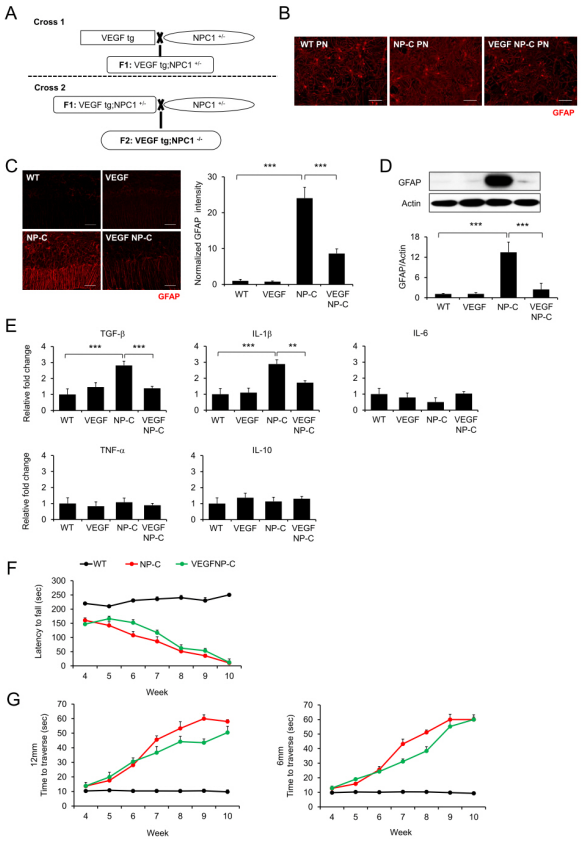

Fig. 3. Improvement of NP-C pathology by replenishment of VEGF. (A) Generation of VEGF/NP-C mice. (B) Representative confocal images of astrocytes activation in cultured cerebellar cells derived from wild-type (WT), NP-C, VEGF, and VEGF/NP-C mice. Scale bar, 50 μm. (C) Representative fluorescence images and quantification of GFAP in cerebellum of wild-type (WT), NP-C, VEGF, and VEGF/NP-C mice (n = 3 per group). Scale bars, 50 μm. (D) Western blot analysis of GFAP in cerebellum of WT, NP-C, VEGF and VEGF/NP-C mice (n = 3 per group). (E) mRNA levels of inflammation related genes in the cerebellum of WT, NP-C, VEGF and VEGF/NP-C mice (n = 3 per group). (F) Rota-rod scores of WT, NP-C and VEGF/NP-C mice (n = 6-7 per group). (G) Beam test of WT, NP-C and VEGF/NP-C mice. Left, 12-mm square beam. Right, 6-mm square beam (n = 6-7 per group). (C-G) One-way analysis of variance, Tukey's post hoc test. **P < 0.01, ***P < 0.001. All error bars indicate standard error of the mean.

DISCUSSION

In the present study, we characterized a conditional null mutation of the mouse VEGF gene, and demonstrated that gene deletion restricted to PNs is sufficient to cause NP-C pathology including astrocyte activation and PNs loss. We also confirmed that replenishment of neuronal VEGF improved NP-C pathology by reducing astrocytes activation. Based on these observations, we propose that VEGF in PNs is the main mediator of excessive astrocyte activation in NP-C, particularly in the cerebellum, and that it could be a new therapeutic target for this disease.

We have previously found that VEGF activity is reduced in NP-C neurons and causes defective autophagy by sphingolipid change related with abnormalities in the VEGF/sphingosine kinase (SphK) pathway, resulting in progressive neuronal loss (2). Glial cells are pivotal to maintain healthy brain function and to protect the brain from damage. Moreover, glial cells play a key role to modulate neuronal activity by regulating synaptic transmission (11). In particular, astrocytes are the most abundant cells in the central nervous system and most likely play an important role in the homeostasis and maintenance of the brain (12). Previous studies have focused on the potential role of astrocytes in relation to the NPC neuropathogenesis, because NPC1 protein is robustly expressed in these cells (13-15). However, recent study demonstrated that mice expressing a tagged *NPC1* transgene

in astrocytes did not rescue NPC phenotype (16). Moreover, astrocyte-specific null mutants displayed no phenotypic abnormalities, histopathological changes, or evidence of synaptic dysfunction and glial activation (17). These works demonstrated that NPC1 deficiency in astrocytes is not sufficient to mediate the disease. Consequently, we thought that astrogliosis was the consequence rather than the cause of neuronal dysfunction and death. Therefore, the present study was designed to determine whether deletion or replenishment of VEGF in PNs was related to NP-C pathology. Here, we showed for the first time that conditional inactivation of VEGF in PNs was sufficient to cause NP-C phenotype, and neuron specific-VEGF overexpression provides greater functional benefit and/or enhances neuroprotection in NP-C.

NP-C is a highly complex lipid storage disorder that leads to progressive deterioration of the nervous system and multiple organ systems in the body (18). Although therapies targeting the deficiency of NPC1 gene/protein are helpful in the treatment of NPC pathologies, it may be difficult to elusive for the time being. Therefore combination of brain and systemic therapy for many downstream targets might play more beneficial role in the improvement of symptoms in NPC patients. The therapeutic approach using a 2-Hydroxypropyl-β-cyclodextrin (CD), which chelates cholesterol, has been demonstrated to ameliorate the disease symptoms in *NPC1*-mutant mice dramatically (19, 20). However, it has clinical limitations in that the blood-brain barrier was shown to be practically non-permeable for CD (21). Thus, many researchers are attempting to overcome the limitations of CD and increase the therapeutic efficacy through combinational therapy with molecules such as miglustat, allopregnanolone, ibuprofen, and curcumin (22, 23). In this study, we showed that VEGF overexpression in the brain led to delayed onset of neurodegeneration and normalization of markers for neuro-inflammation, ultimately leading to improved behavior. Combination therapy focused on VEGF together with CD treatment may be synergistic, and could be investigated in the future.

MATERIALS AND METHODS

Animals

A colony of BALB/c *NPC1*^{nih} mice (NP-C mice) has been maintained for this study by brother-sister mating of heterozygous animals. L7/Pcp2-cre (7), *NPC1*$^{flox/flox}$ (8) or VEGF$^{flox/flox}$ mice (24) were used to delete the *NPC1* gene or VEGF in PNs, respectively. Polymerase chain reaction (PCR) was performed for determining the genotype of each mouse (2). Transgenic mice overexpressing VEGF (25) in the brain under the control of neuron-specific promoters were bred with NP-C mice to generate VEGF/NP-C (VEGFtg/*NPC1*$^{-/-}$) mice. We choose the block randomization method to allocate the animals to experimental groups. To eliminate the bias, we were blinded to the experimental groups during data collection and analysis Mice were housed under a 12-hour day-night cycle with free access to tap water and food pellets. All mouse studies were approved by the Kyungpook National University Institutional Animal Care and Use Committee (IACUC).

Behavioral tests

We performed behavioral analyses to assess balance and coordination by measuring the amount of time the mice were able to remain on a longitudinally rotating rod. Briefly, the Rota-rod apparatus (Ugo Basile) was set to an initial speed of four rotations per minute (rpm), and the acceleration was increased by 32 rpm every 25-30 s. The latency to fall was measured in each trial for a total duration of 5 min. Scores were registered every 7 days, and three independent tests were performed at each measurement. Motor coordination, balance, and hindlimb placement were evaluated by assessing the ability of mice to cross two types of balance beams to reach a safety platform. Each mouse was tested for its ability to traverse two different styles of 41-cm-long scored Plexiglas beams. One was 12 mm in diameter, and the other was 6 mm wide. Beams were placed horizontally 50 cm above a table. Time to traverse each beam was recorded for each trial with a 60-s maximum cutoff, and falls were scored as 60 s. Scores were registered every 7 days.

Isolation and culture of cerebellar cells

Dissociated cerebellar cell cultures were prepared from individual embryonic (E) day 18 fetuses, namely WT, NP-C, and VEGF/NP-C (identified by PCR) as previously described (26) with some minor modifications. Briefly, the entire cerebellum was removed and kept in ice-cold Hank's balance salt solution containing gentamicin (10 μg/ml, GIBCO). Each cerebellum was then dissociated into single cells using the SUMITOMO Nerve-Cell Culture System (Sumitomo Bakelite), and the cells were resuspended in seeding medium (Minimum Essential Medium; GIBCO) supplemented with L-glutamine (4 mM), D-glucose (11 mM), sodium pyruvate (500 μM), gentamicin (10 μg/ml), and 10% heat-inactivated fetal bovine serum. The cell suspensions were seeded on poly-L-ornithine-coated (Sigma-Aldrich) glass coverslips (12 mm) at a density of 5×10^6 cells per milliliter, with each coverslip in an individual well of a 24-well tissue culture plate. After 3 h of incubation in a CO_2 incubator, 1 ml of culture medium further supplemented with B-27 supplement (GIBCO), N2 supplement (GIBCO), bovine serum albumin (100 μg/ml, Sigma-Aldrich), and tri-iodothyronine (0.5 nM; Sigma-Aldrich) was added to each culture well. After 7 days, half of the medium in each well was replaced with fresh culture medium. For some experiments, cells were treated with mouse SMART pool VEGF siRNA (Dharmacon) or scrambled sequence siRNA control (Dharmacon).

Lentiviral shRNA-mediated depletion of VEGF

We cloned VEGF shRNAs into lentiviral vector plasmid CS-CDF-CG-PRE. The following short hairpin sequences were

Table 1. Sequences of primer pairs

Gene	Forward	Reverse
TNF-α	5′-GAT TAT GGC TCA GGG TCC AA-3′	5′-GCT CCA GTG AAT TCG GAA AG-3′
IL-1β	5′-CCC AAG CAA TAC CCA AAG AA-3′	5′-GCT TGT GCT CTG CTT GTG AG-3′
IL-6	5′-CCG GAG AGG AGA CTT CAC AG-3′	5′-TTG CCA TTG CAC AAC TCT TT-3′
IL-10	5′-AAG GCC ATG AAT GAA TTT GA-3′	5′-TTC GGA GAG AGG TAC AAA CG-3′
TGF-β	5′-CAC CCA CTT TTG GAT CTC AG-3′	5′-CCC AAG GAA AGG TAG GTG AT-3′
GAPDH	5′-TGA ATA CGG CTA CAG CAA CA-3′	5′-AGG CCC CTC CTG TTA TTA TG-3′

used: 5′-GATGTGAATGCAGACCAAAGA-3′ (SABiosciences-Qiagen; KM03041N; VEGF-shRNA #4) and 5′-GGAATCTCA TTCGATGCATAC-3′ (SABiosciences-Qiagen; negative control shRNA). The shRNA-expressing lentiviruses were produced by transient transfection of 293T cells. Virus-containing media were collected, filtered, and concentrated by ultracentrifugation at 50,000 g for 2 h and resuspended in phosphate buffered saline (PBS). Viral titers were measured by serial dilution on 293T cells, followed by flow cytometry analysis after 48 h. The titer of the virus used ranged between 2 and 5 $\times 10^9$ plaque-forming units per ml. Using stereotaxic injections, 3 μl of lentiviruses were administered into the cerebellum of 4-week-old mice at 3 days before analysis, as previously described (2).

Immunofluorescence staining

For the immunofluorescence staining, brain sections were blocked with PBS containing 5% normal goat serum (Vector Laboratories), 2% BSA (GIBCO) and 0.4% Triton X-100 (Sigma-Aldrich). In the same buffer solution, sections were then incubated for 24 h with primary antibodies. The following primary antibodies were used: anti-calbindin (rabbit, 1:500, Chemicon, ab82812) and anti-GFAP (rabbit, diluted 1:500; DAKO). For visualization, sections were incubated in secondary antibodies for 2 h at room temperature followed by washes. Alexa Fluor 488 or 594-conjugated goat anti-rabbit IgG (1:1,000, Molecular Probes, Carlsbad, CA) was used as secondary antibody. The sections were analyzed with a laser scanning confocal microscope equipped with Fluoview SV1000 imaging software (Olympus FV1000) or with an Olympus BX51 microscope. Metamorph software (Molecular Devices) was used to calculate the average intensity.

Western blotting

The brain tissues were weighed and sonicated in 10X volume of RIPA buffer plus protease inhibitors. Equal amounts of protein samples (~80 μg) in SDS sample buffer were subjected to sodium dodecyl sulfate polyacrylamide gel electrophoresis and transferred electrophoretically to immunoblotting polyvinylidene difluoride membranes. The membranes were pretreated with blocking solution (5% skim milk, 0.1% Tween 20 in PBS) for 1 h at room temperature and incubated with primary antibodies against GFAP (rabbit, 1:500, Dako, N1506) and β-actin (1:1,000; Santa Cruz Biotechnology) in blocking solution overnight at 4°C. They were then washed with a washing solution (0.1% Tween-20 in PBS) five times for 10 min each and incubated with horseradish peroxidase-conjugated secondary antibodies against rabbit IgG in blocking solution for 1 h. Subsequently, the membranes were washed again five times for 10 min each, and the protein signals were detected by chemiluminescence exposed to x-ray film. Densitometric quantification was performed using the ImageJ software (National Institutes of Health).

RNA isolation and real-time PCR analysis

RNA was extracted using the RNeasy Lipid Tissue Mini kit (QIAGEN) according to the manufacturer's instructions. cDNA was synthesized from 5 μg of total RNA using a commercially available kit (Takara Bio Inc.). Quantitative real-time PCR was performed using a Corbett research RG-6000 real-time PCR instrument. Used primers are described in Table 1.

Statistical analysis

Results are expressed as mean ± standard error of the mean (SEM). Comparisons between two groups were performed with Student's *t*-test. In cases where more than two groups were compared to each other, a one way analysis of variance (ANOVA) was used, followed by Tukey's HSD test. All statistical analysis was performed using SPSS statistical software. $P < 0.05$ was considered to be significant.

ACKNOWLEDGEMENTS

This research was supported by a grant of the Korea Health Technology R&D Project through the Korea Health Industry Development Institute (KHIDI), funded by the Ministry of Health & Welfare, Republic of Korea (grant number: HI17HI17C2140) and the National Research Foundation of Korea (NRF) grant funded by the Korea government (MSIP) (2017R1A4A1015652).

CONFLICTS OF INTEREST

The authors have no conflicting interests.

REFERENCES

1. Vanier MT and Millat G (2003) Niemann-Pick disease type C. Clin Genet 64, 269-281
2. Lee H, Lee JK, Park MH et al (2014) Pathological roles of the VEGF/SphK pathway in Niemann-Pick type C neurons. Nat Commun 5, 5514
3. Pentchev PG, Comly ME, Kruth HS et al (1985) A defect in cholesterol esterification in Niemann-Pick disease (type C) patients. Proc Natl Acad Sci U S A 82, 8247-8251
4. Karten B, Vance DE, Campenot RB and Vance JE (2002) Cholesterol accumulates in cell bodies, but is decreased in distal axons, of Niemann-Pick C1-deficient neurons. J Neurochem 83, 1154-1163
5. Sarna JR, Larouche M, Marzban H, Sillitoe RV, Rancourt DE and Hawkes R (2003) Patterned Purkinje cell degeneration in mouse models of Niemann-Pick type C disease. J Comp Neurol 456, 279-291
6. Bae JS, Furuya S, Ahn SJ, Yi SJ, Hirabayashi Y and Jin HK (2005) Neuroglial activation in Niemann-Pick Type C mice is suppressed by intracerebral transplantation of bone marrow-derived mesenchymal stem cells. Neurosci Lett 381, 234-236
7. Zhang XM, Ng AH, Tanner JA et al (2004) Highly restricted expression of Cre recombinase in cerebellar Purkinje cells. Genesis 40, 45-51
8. Elrick MJ, Pacheco CD, Yu T et al (2010) Conditional Niemann-Pick C mice demonstrate cell autonomous Purkinje cell neurodegeneration. Hum Mol Genet 19, 837-847
9. Lange C, Storkebaum E, de Almodóvar CR, Dewerchin M and Carmeliet P (2016) Vascular endothelial growth factor: a neurovascular target in neurological diseases. Nat Rev Neurol 12, 439-454
10. Licht T, Goshen I, Avital A et al (2011) Reversible modulations of neuronal plasticity by VEGF. Proc Natl Acad Sci U S A 108, 5081-5086
11. Giaume C, Kirchhoff F, Matute C, Reichenbach A and Verkhratsky A (2007) Glia: the fulcrum of brain diseases. Cell Death Differ 14, 1324-1335
12. Nimmerjahn A (2009) Astrocytes going live: advances and challenges. J Physiol 587, 1639-1647
13. Baudry M, Yao Y, Simmons D, Liu J and Bi X (2003) Postnatal development of inflammation in a murine model of Niemann-Pick type C disease: immunohistochemical observations of microglia and astroglia. Exp Neurol 184, 887-903
14. German DC, Liang CL, Song T, Yazdani U, Xie C and Dietschy JM (2002) Neurodegeneration in the Niemann-Pick C mouse: glial involvement. Neuroscience 109, 437-450
15. Patel SC, Suresh S, Kumar U et al (1999) Localization of Niemann-Pick C1 protein in astrocytes: implications for neuronal degeneration in Niemann- Pick type C disease. Proc Natl Acad Sci U S A 96, 1657-1662
16. Lopez ME, Klein AD, Dimbil UJ and Scott MP (2011) Anatomically defined neuron-based rescue of neurodegenerative Niemann-Pick type C disorder. J Neurosci 31, 4367-4378
17. Yu T, Shakkottai VG, Chung C and Lieberman AP (2011) Temporal and cell-specific deletion establishes that neuronal Npc1 deficiency is sufficient to mediate neurodegeneration. Hum Mol Genet 20, 4440-4451
18. Vanier MT (2010) Niemann-Pick disease type C. Orphanet J Rare Dis 5, 16
19. Davidson CD, Ali NF, Micsenyi MC et al (2009) Chronic cyclodextrin treatment of murine Niemann-Pick C disease ameliorates neuronal cholesterol and glycosphingolipid storage and disease progression. PLoS One 4, e6951
20. Lopez AM, Terpack SJ, Posey KS, Liu B, Ramirez CM and Turley SD (2014) Systemic administration of 2-hydroxypropyl-β-cyclodextrin to symptomatic Npc1-deficient mice slows cholesterol sequestration in the major organs and improves liver function. Clin Exp Pharmacol Physiol 41, 780-787
21. Camargo F, Erickson RP, Garver WS et al (2001) Cyclodextrins in the treatment of a mouse model of Niemann-Pick C disease. Life Sci 70, 131-142
22. Hovakimyan M, Maass F and Petersen J (2013) Combined therapy with cyclodextrin/allopregnanolone and miglustat improves motor but not cognitive functions in Niemann-Pick Type C1 mice. Neuroscience 252, 201-211
23. Williams IM, Wallom KL, Smith DA, Al Eisa N, Smith C, Platt FM (2014) Improved neuroprotection using miglustat, curcumin and ibuprofen as a triple combination therapy in Niemann-Pick disease type C1 mice. Neurobiol Dis 67, 9-17
24. Gerber HP, Hillan KJ, Ryan AM et al (1999) VEGF is required for growth and survival in neonatal mice. Development 126, 1149-1159
25. Wang Y, Kilic E, Kilic U et al (2005) VEGF overexpression induces post-ischaemic neuroprotection, but facilitates haemodynamic steal phenomena. Brain 128, 52-63
26. Tabata T, Sawada S, Araki K, Bono Y, Furuya S and Kano M (2000) A reliable method for culture of dissociated mouse cerebellar cells enriched for Purkinje neurons. J Neurosci Methods 104, 45-53